ACS APPLIED MATERIALS & INTERFACES

Research Article

www.acsami.org

Titania Composite Microspheres Endowed with a Size-Exclusive Effect toward the Highly Specific Revelation of Phosphopeptidome

Ying Zhang,[†,‡] Wanfu Ma,[§,‡] Cheng Zhang,[†] Changchun Wang,*[,§] and Haojie Lu*[,†]

[†]Department of Chemistry and Institutes of Biomedical Sciences, Fudan University, Shanghai 200032, China

[§]State Key Laboratory of Molecular Engineering of Polymers and Department of Macromolecular Science, Laboratory of Advanced Materials, Fudan University, Shanghai 200433, China

Supporting Information

ABSTRACT: The efficient isolation of low-abundance phosphopeptides from complicated biological samples containing a significant quantity of nonphosphopeptides and proteins is essential for phosphopeptidome research but remains a great challenge. In this Article, magnetic composite microspheres comprising a magnetic colloidal nanocrystal cluster core and a mesoporous titania shell with an average pore diameter of 3.4 nm were modified by directly coating an amorphous titania shell onto the magnetite core, followed by converting the amorphous titania shell into a crystalline structure via a hydrothermal process at 80 °C. The as-prepared magnetic mesoporous titania microspheres possess a remarkable specific surface area that is as high as 603.5 m^2/g, which is an appropriate pore size with a narrow size distribution and a high magnetic responsiveness. These outstanding features imply that the composite microspheres exhibit extraordinary performance in phosphopeptidome research, including high specificity toward phosphopeptides, an excellent size-exclusion effect against phosphoproteins, exceptional enrichment capacity, and efficient separation from mixtures. Encouraged by the experimental results, we employed this method to investigate the phosphopeptidome of snake venom for the first time. A total of 35 phosphopeptides was identified from the snake venom from the family Viperidae, accounting for 75% of the total identified peptides. This result represents the largest data set of the phosphopeptidome in snake venom from the family Viperidae.

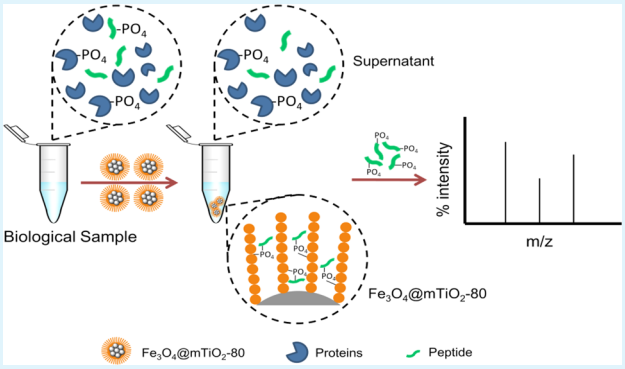

KEYWORDS: *magnetic composite microspheres, mesoporous titania, hydrothermal process, size-exclusion effect, phosphopeptidome*

1. INTRODUCTION

Since MCM-41 and SBA-15 were first reported in the 1990s, mesoporous materials have been extensively investigated due to their high specific surface area, large pore volume, appropriate pore size, and wide range of applications;[1−10] significant efforts have been made to synthesize novel mesoporous materials for proteomics research.[11−16] To date, numerous types of mesoporous materials, such as mesoporous silicas,[11,12] mesoporous carbons,[15] and metal organic frameworks,[16] have been explored to extract peptides with low abundances from complicated biological samples. Magnetic nanocomposites have achieved great success in bioseparation because of their unique magnetic responsiveness and designed functionalities.[17−20] As an important member of this class, magnetic mesoporous composite microspheres synthesized via entrapping magnetically responsive cores in a mesoporous matrix have the ability to simultaneously achieve easy and effective isolation of the target biomolecules.[21−27]

Compared with proteins, biologically active peptides (with molecular weights of less than 10 kDa) are sufficiently small to enter body fluid passively and produce diagnostic traces as a result of protein synthesis, processing, and degradation. Therefore, these naturally existing peptides, called peptidome, have drawn increasing attention from scientists.[28] Comprehensive analysis of peptidomes in complex biological mixtures can contribute to a better understanding of biological functions and the discovery of novel biomarkers with higher sensitivity and specificity.[29,30] Phosphopeptidomes, the naturally existing phosphopeptides in biological samples and an important subset of peptidome, modulate a wide range of biological functions and protein activities.[31] Although the development of functional materials has promoted the research of the phosphoproteome, the state-of-art techniques for enriching the phosphoproteome are not suitable for the extraction of the phosphopeptidome because there exists a fundamental difference between phosphoproteome and phosphopeptidome extraction. In conventional phosphoproteome research, all of the proteins are first digested into a mixture of nonphosphopeptides and phosphopeptides. The digestion process is employed to generate phosphopeptides for the confirmation

Received: October 25, 2013
Accepted: April 18, 2014
Published: April 18, 2014

   dx.doi.org/10.1021/am501339e | ACS Appl. Mater. Interfaces 2014, 6, 6290−6299

of phosphorylated sites because the identification of phosphorylated sites at the protein level is significantly more difficult. Phosphopeptides are then selectively enriched from a pool containing a large set of peptides using functional materials to avoid the interference of nonphosphopeptides. Because the proteins are digested into peptides, most of the reported phosphoproteome enrichment materials, including that presented in our previous work,[25] do not require a size-exclusion effect against proteins. In contrast, because additional phosphopeptides are generated from the digestion of the phosphoproteins, a digestion process cannot be used in phosphopeptidome research. For this reason, large amounts of proteins, including phosphoproteins, exist in the test samples, and their presence significantly hampers the mass spectrometric analysis of the phosphopeptides.[32] Therefore, the efficient isolation of phosphopeptides from complex samples containing high concentrations of proteins, including both nonphosphoproteins and phosphoproteins, is the most important prerequisite for successful phosphopeptidome research.

Recent advances in mesoporous nanomaterials for the solid-phase extraction of peptidomes based on a size-exclusion mechanism have shed new light into peptidome research.[15,33−38] Mesoporous nanomaterials, including MCM-41, etc., with highly ordered channels and controllable pore entrance radii, have demonstrated great promise in addressing the size-exclusion issues. To selectively capture the phosphopeptidome, a Ti^{4+}-functionalized mesoporous material was synthesized with both a size-exclusion effect and phosphopeptide-specific selectivity and was then successfully applied to phosphopeptidome research.[39] However, the relatively low density of the surface functional group decreased the specificity of this material toward phosphopeptides. Compared with metal ions immobilized on mesoporous silica, mesoporous metal oxide architectures combining both the characteristics of a mesoporous structure and a metal oxide surface are particularly fascinating because of their molecular cutoff effects, highly pure interface, and abundant interaction sites toward the specific retention of phosphopeptides.

In this work, we report a simple and effective method for the extraction of phosphopeptidomes using custom-made, magnetic, mesoporous titania composite microspheres endowed with size-exclusion effects. The unique properties of this material for phosphopeptidome enrichment include (1) a highly pure and crystalline interface that is responsible for high specificity toward phosphopeptides, (2) an appropriate pore diameter (ca. 3 nm) and a narrow pore-size distribution, both of which ensure the effective exclusion of nonphosphoproteins and phosphoproteins, (3) ultra-high specific surface area (>600 m^2/g) providing a high enrichment capacity for phosphopeptides, and (4) a high-magnetic-response magnetite core, which enables the convenient removal of phosphopeptides from a pool that consists predominantly of other proteins and nonphosphopeptides by applying an external magnetic field after enrichment.

2. EXPERIMENTAL SECTION

2.1. Materials. Iron(III) chloride hexahydrate ($FeCl_3·6H_2O$), ammonium acetate (NH_4OAc), ethylene glycol (E.G.), anhydrous ethanol, trisodium citrate dehydrate, and aqueous ammonia solution (25%) were purchased from Shanghai Chemical Reagents Company (Shanghai, China) and used as received. β-Casein, bovine serum albumin, asialofetuin, 2,5-dihydroxybenzoic acid (2,5-DHB, 98%), ammonium bicarbonate (ABC, 99.5%), and 1-1-(tosylamido)-2-phenyl-ethyl chloromethyl ketone (TPCK)-treated trypsin (E.G 2.4.21.4) were purchased from Sigma (St. Louis, MO). A lyophilized powder of snake venom from the family Viperidae was obtained from Xinyuan Venom Distribution Division (Guangzhou, China). Acetonitrile (ACN, 99.9%) and trifluoroacetic acid (TFA, 99.8%) were purchased from Merck (Darmstadt, Germany). Phosphoric acid (85%) was purchased from Shanghai Feida Chemical Reagents Ltd. (Shanghai, China). DHB matrix was dissolved in an acetonitrile (ACN)/water (50/50, v/v) solution containing 1% H_3PO_4, and DHB was maintained at 10 $mg·mL^{-1}$. Deionized water (18.4 MΩ cm) was used for all experiments and was obtained from a Milli-Q system (Millipore, Bedford, MA).

2.2. Preparation of MCNCs Stabilized by Citrate. Magnetite colloidal nanocrystal clusters (MCNCs) were prepared using a modified solvothermal reaction.[40] Typically, $FeCl_3·6H_2O$ (1.350 g), NH_4Ac (3.854 g), and sodium citrate (0.4 g) were dissolved in ethylene glycol (70 mL). The mixture was stirred vigorously for 1 h at 170 °C to form a homogeneous black solution, which was then transferred to a Teflon-lined, stainless-steel autoclave (a capacity of 100 mL). The autoclave was heated at 200 °C and stored for 16 h before cooling to room temperature. The black product was washed with ethanol and collected using a magnet. The cycle of washing and magnetic separation was repeated several times. The final product was dispersed in ethanol for further use.

2.3. Preparation of Fe_3O_4@TiO_2 Core/Shell Microspheres. The Fe_3O_4@TiO_2 core/shell microspheres were synthesized by directly coating a TiO_2 layer on the surface of the MCNCs in a mixed solvent of ethanol and acetonitrile at room temperature by hydrolyzing TBOT in the presence of ammonia. Briefly, the as-prepared MCNCs (50 mg) were dispersed in a mixed solvent containing ethanol (75 mL) and acetonitrile (25 mL) with the aid of an ultrasonicator; the solution was then mixed with $NH_3·H_2O$ (0.5 mL) at room temperature. Finally, a solution of TBOT (1 mL) in ethanol (15 mL) and acetonitrile (5 mL) was added to the above suspension under stirring. After reacting for 1.5 h, the products were collected using magnetic separation and were then washed multiple times with ethanol and acetonitrile.

2.4. Preparation of Fe_3O_4@mTiO_2 Core/Shell Microspheres. Mesoporous TiO_2 shells were synthesized by treating Fe_3O_4@TiO_2 microspheres with a hydrothermal method. Typically, the as-synthesized Fe_3O_4@TiO_2 microspheres were dispersed in 60 mL of mixed solvent containing ethanol (40 mL) and deionized water (20 mL). The mixture was then transferred to a Teflon-lined, stainless-steel autoclave (capacity of 100 mL). The autoclave was heated at a certain temperature and maintained for 20 h. Then, the mixture was cooled to room temperature, and the resulting black product was washed with ethanol and collected using a magnet.

2.5. Preparation of Tryptic Digests of Standard Proteins. β-Casein and BSA were dissolved in ABC (25 mM) at pH 8.0 (1 mg/mL for each protein) and denatured by boiling for 10 min. The protein solutions were then incubated with trypsin at an enzyme/substrate ratio of 1:40 (w/w) for 12 h at 37 °C to produce proteolytic digests. The tryptic peptide mixtures were stored at −20 °C until further use.

2.6. Characterization. Field-emission transmission electron microscopy (FE-TEM) images were collected using a JEM-2100F transmission electron microscope at an acceleration voltage of 200 kV. The samples were dispersed at an appropriate concentration and cast onto a carbon-coated copper grid. Magnetic characterization was carried out using a vibrating sample magnetometer (VSM) on a Model 6000 physical property measurement system (Quantum, USA) at 300 K. X-ray diffraction (XRD) patterns were collected on an X'Pert Pro (Panalytical, The Netherlands) diffractometer with Cu KR radiation at λ = 0.154 nm operating at 40 kV and 40 mA. Nitrogen adsorption−desorption measurements were performed on an ASAP2020 (Micromeritics, USA) accelerated surface area analyzer at 77 K. Before obtaining the measurements, the samples were degassed in a vacuum at 120 °C for at least 6 h.

2.7. Selective Enrichment of Phosphopeptides with Fe_3O_4@mTiO_2-80. The obtained Fe_3O_4@mTiO_2-80 was first washed with

Scheme 1. Schematic Illustration of the Synthetic Procedures for the Preparation of Modified Fe_3O_4@$mTiO_2$-80

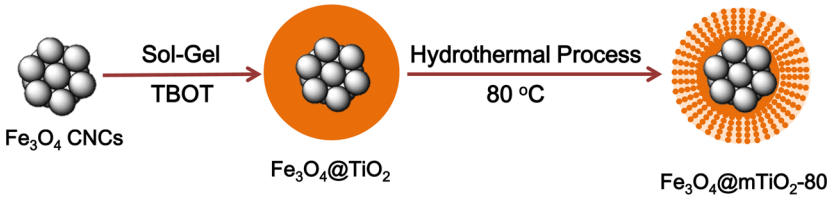

ethanol three times and then suspended in deionized water (10 mg·mL^{-1}). Tryptic digests of β-casein and BSA were dissolved in loading buffer (50% ACN containing 5% TFA, 100 μL), and then, Fe_3O_4@$mTiO_2$-80 (2 μL) was added and incubated at room temperature. Subsequently, Fe_3O_4@$mTiO_2$-80 with captured phosphopeptides was separated from the mixed solution by applying an external magnet. After washing with loading buffer (200 μL) to remove the nonspecifically adsorbed peptides, the trapped phosphopeptides were eluted with $NH_3{\cdot}H_2O$ (5%, 10 μL) for further MS analysis. The enrichment of phosphopeptides from protein mixtures was the same as described above, i.e., the protein mixture contained BSA (protein)/β-casein (protein)/β-casein digests at a mass ratio of 100:100:1.

2.8. Investigation of the Size Exclusion Effect of Fe_3O_4@$mTiO_2$-80 Core/Shell Microspheres. Asialofetuin and β-casein protein standards were dissolved in a buffer solution (50% ACN containing 5% TFA, 20 ng·μL^{-1}). To determine the quantity of adsorbed proteins, Fe_3O_4@$mTiO_2$-80 aqueous suspensions (10 mg·mL^{-1}, 2 μL) were added to the protein solutions (100 μL). Then, the suspensions were incubated with shaking at R.T., followed by the separation of Fe_3O_4@$mTiO_2$-80 using an external magnetic field. The supernatants were collected and lyophilized for ultraviolet (UV) analysis. The relative amounts of the proteins before and after adsorption were compared by measuring the differences in the protein concentration using the bicinchoninic acid method.

2.9. Enrichment of Phosphopeptidome from Snake Venom. The enrichment procedure for the phosphopeptidome from snake venom using Fe_3O_4@$mTiO_2$-80 was the same as that described for the phosphopeptide enrichment of the standard samples.

2.10. MALDI Mass Spectrometry. MALDI mass spectrometric analysis was performed to analyze the phosphopeptides enriched from the standard samples. The eluent (1 μL) was deposited on the MALDI probe, and then, the DHB matrix solution (1 μL) was deposited for MS analysis. MALDI-TOF-MS analysis was performed in positive reflection mode on a 5800 Proteomic Analyzer (Applied Biosystems, Framingham, MA, USA) using a Nd:YAG laser at 355 nm, a repetition rate of 200 Hz, and an acceleration voltage of 20 kV. The range of laser energy was optimized to obtain good resolution and signal-to-noise ratio (S/N) and was held constant for further analysis. An external mass calibration was performed using standard peptides from myoglobin digests.

2.11. 1D Nano-Flow Liquid Chromatography-Tandem MS (LC-MS/MS) Analysis. Phosphopeptides enriched from snake venom were analyzed using 1D nano-flow LC-MS/MS. Liquid chromatography was performed on a nano Acquity UPLC system (Waters Corporation, Milford, USA) connected to a LTQ Orbitrap XL mass spectrometer (Thermo Scientific, Bremen, Germany) equipped with an online nano-electrospray ion source (Michrom Bioresources, Auburn, USA). Peptides were resuspended in solvent A (2% acetonitrile, 0.1% formic acid in water, 25 μL). Peptide solution (20 μL) was loaded onto the Captrap Peptide column (2 mm × 0.5 mm, Michrom Bioresources, Auburn, USA) at a flow rate of 20 $\mu L\ min^{-1}$ of solvent A for 5 min and then separated on a Magic C18AQ reverse-phase column (100 μm id × 15 cm, Michrom Bioresources, Auburn, USA) with a linear gradient, starting from 5% B (90% acetonitrile, 0.1% formic acid in water) and increasing to 45% B (that is, from 95% A to 55% A, the same below) for 100 min. The column flow rate was maintained at 500 nL min^{-1}. The electrospray voltage (1.6 kV) versus the inlet of the mass spectrometer was used. The LTQ Orbitrap XL mass spectrometer was operated in the data-dependent mode to switch automatically between MS and MS/MS acquisition. A full survey scan of the MS spectrum using one microscan (m/z 350–1800) was acquired in the Obitrap with a mass resolution of 60,000 at m/z 400, followed by MS/MS of the eight most-intense peptide ions in the LTQ analyzer. The automatic gain control (AGC) was set to 10^6 ions with a maximum accumulation time of 500 ms. Single charge states were rejected, and dynamic exclusion was used with two microscans with exclusion durations of 15 and 30 s. For MS/MS, precursor ions were activated using 35% normalized collision energy at the default activation, q, of 0.25 and an activation time of 30 ms. The mass spectrometer was set so that one full MS scan was followed by three MS2 scans and three neutral loss MS3 scans. Phosphopeptide detection was performed by setting the mass spectrometer to acquire a full MS scan, followed by three data-dependent MS2 scans. Subsequently, an MS3 spectrum was automatically triggered when the three most intense peaks from the MS2 spectrum corresponded to a neutral loss event of 98, 49, and 32.67 ± 1 Da for the precursor ion with 1+, 2+, and 3+ charge states, respectively. The spectra were recorded using Xcalibur (version 2.0.7) software.

2.12. Data Processing and Analysis. All of the MS/MS spectra in the raw files were converted to single *.mgf files using MassMatrix Mass Spectrometric Data File Conversion Tools (version 3.9, http://www.massmatrix.net/download). The *.mgf files were searched using the Mascot Daemon software (Version 2.3.0, Matrix Science, London, UK) based on the Mascot algorithm. The database used for searching was the UniProtKB/Swiss-Prot database (Taxonomy: vipera; release 2013_04_25, with 142 entries). The searching parameters were set as follows: peptides were searched without the specification of cleavage enzymes. Oxidation on methionine (15.9949 Da) was set as a variable modification. The peptide mass tolerance was 20 ppm, and the fragment ion tolerance was 1.0 Da. Peptide identifications were considered for expectation values lower than 0.05 ($p < 0.05$). The expectation cutoff value of 0.05 was applied in the MASCOT ion score to avoid selecting peptide identifications out of the 95% confidence interval.

3. RESULTS AND DISCUSSION

3.1. Preparation and Characterization of Fe_3O_4@$mTiO_2$-80 with Ultra-High Specific Surface Area and Appropriate Pore Size. The protocol employed for the preparation of magnetic mesoporous titania composite microspheres endowed with a size-exclusion effect is schematically illustrated in Scheme 1. Briefly, magnetite colloidal nanocrystal clusters (MCNCs) stabilized by sodium citrate were first synthesized using a modified solvothermal reaction. A sol–gel process was then carried out to encapsulate the MCNCs in a compact and amorphous titania shell. Finally, the Fe_3O_4@TiO_2 microspheres were subjected to a hydrothermal process at 80 °C in a mixed solvent containing ethanol and deionized water at a volume ratio of 2:1, which led to the formation of the modified Fe_3O_4@$mTiO_2$-80. The reaction temperature in the hydrothermal process step is critical for the synthesis of the desired products. When the temperature is relatively high, such as 160 °C (the product we have previously reported is marked as Fe_3O_4@$mTiO_2$-160[25]) or 120 °C (the product is marked as Fe_3O_4@$mTiO_2$-120), magnetic mesoporous titania microspheres with larger pore sizes were obtained. As observed in our previous report and Figure 1, the specific surface areas of

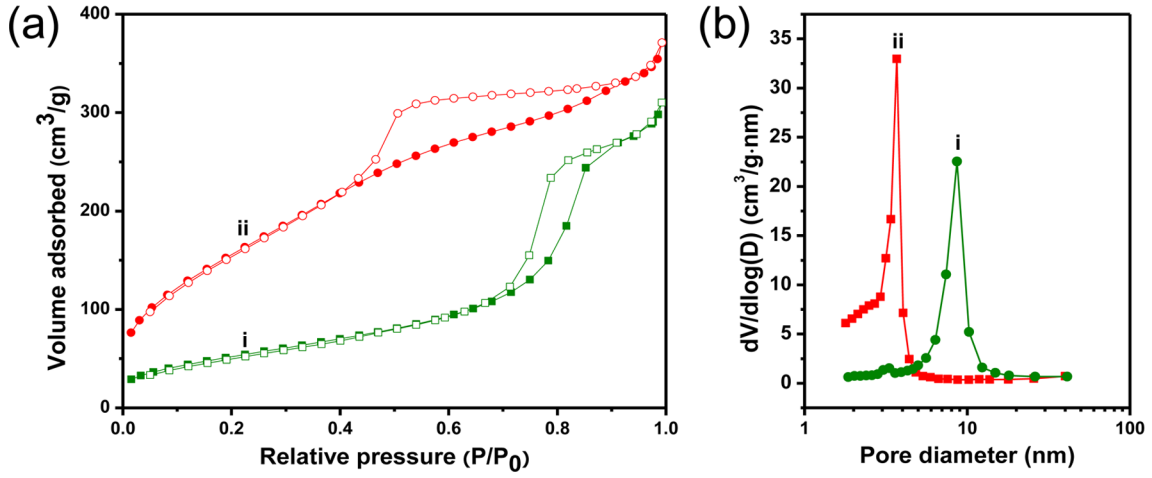

Figure 1. (a) Nitrogen adsorption−desorption isotherms (■ = adsorption, □ = desorption) and (b) BJH pore-size distribution curves for (i) Fe_3O_4@mTiO_2-120 and (ii) Fe_3O_4@mTiO_2-80.

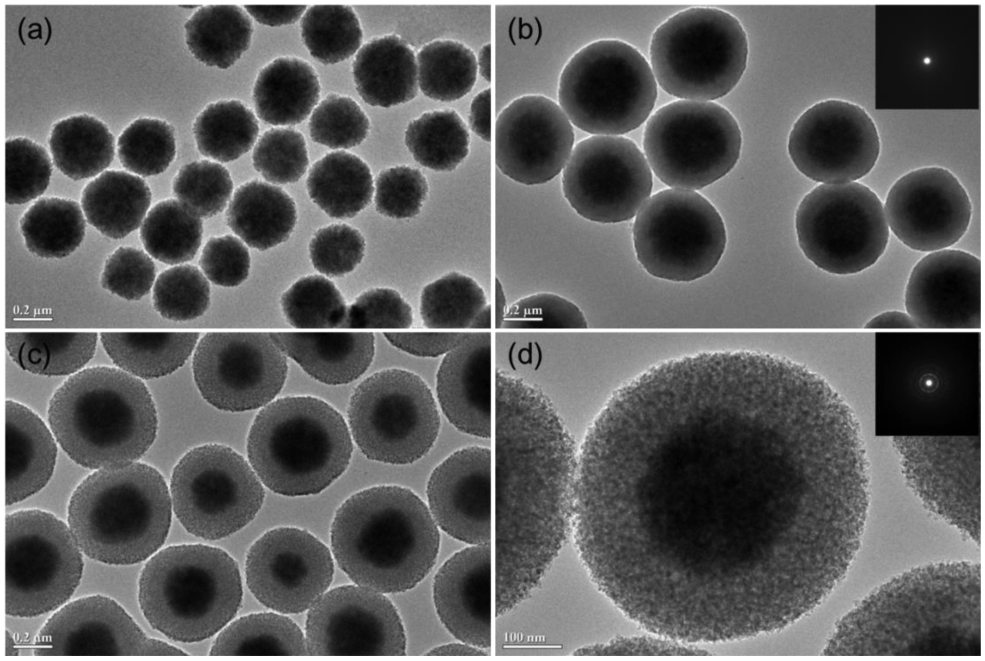

Figure 2. Representative TEM images of (a) MCNCs, (b) Fe_3O_4@TiO_2, and (c, d) Fe_3O_4@mTiO_2-80. (The scale bars are 200 nm for a, b, and c and 100 nm for d).

the resulting Fe_3O_4@mTiO_2 are 167.1 and 194.4 m^2/g, while the average pore sizes are 8.6 and 7.9 nm for Fe_3O_4@mTiO_2-160 and Fe_3O_4@mTiO_2-120, respectively. These microspheres can selectively enrich phosphopeptides for phosphoproteome research. However, they cannot be applied in a phosphopeptidome study because the pores are too large to exclude the phosphoproteins from the phosphopeptides. Decreasing the pore size to approximately 3 nm is highly desirable for efficiently blocking the phosphoproteins while allowing the phosphopeptides to penetrate into the pore channels.[11,33] The pore size of the as-synthesized Fe_3O_4@mTiO_2 could achieve this goal only if the temperature is 80 °C. The porosity properties of Fe_3O_4@mTiO_2-80 were characterized using nitrogen adsorption−desorption measurements. As shown in Figure 1, the specific surface area of Fe_3O_4@mTiO_2-80 is as high as 603.5 m^2/g, which is approximately the largest surface area reported for titanium-dioxide-based nanomaterials. Additionally, the relatively uniform pore sizes with average pore diameters of approximately 3.4 nm and a very narrow pore-size distribution fulfill the requirements of the size exclusion effect.

Encouraged by the outstanding features of Fe_3O_4@mTiO_2-80, we used transmission electron microscopy (TEM) characterization to track the entire reaction process. Representative TEM images of each step are shown in Figure 2. First, sodium citrate-stabilized MCNCs with nearly spherical morphologies and average diameters of approximately 280 nm were observed. After encapsulation with an amorphous titania shell, a well-defined core/shell structure could be clearly observed, and the thickness of the titania shell was approximately 120 nm. The TEM image (Figure 2b) and selected-area electron diffraction (SAED) pattern (Figure 2b inset) recorded from a certain area of individual microspheres revealed that the TiO_2 shell was continuous and amorphous. Upon further hydrothermal treatment at a temperature of 80

dx.doi.org/10.1021/am501339e | ACS Appl. Mater. Interfaces 2014, 6, 6290−6299

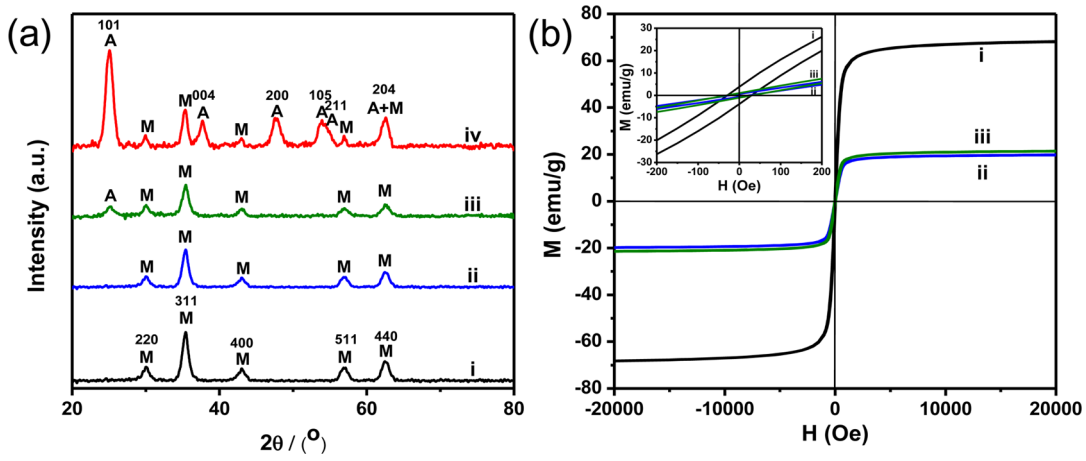

Figure 3. (a) XRD patterns and (b) magnetic hysteresis curves (the inset was the magnified scale of the plot) of (i) MCNCs, (ii) Fe_3O_4@TiO_2, (iii) Fe_3O_4@mTiO_2-80, and (iv) Fe_3O_4@mTiO_2-120.

Scheme 2. Schematic Illustration of the Typical Procedure for Selectively Removing Phosphopeptides from a Sample Containing Large Amounts of Proteins and Nonphosphopeptides Using Fe_3O_4@mTiO_2-80 and Magnetic Separation

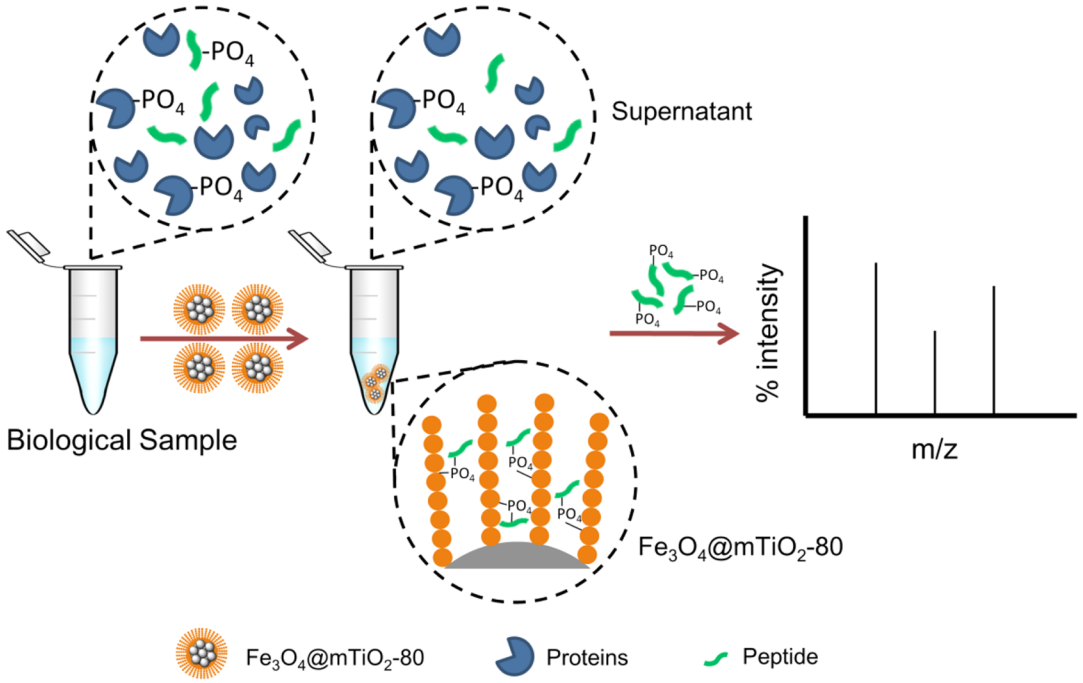

°C, the TiO_2 layer was no longer continuous but constructed from many very small nanocrystals (Figure 2c). Additionally, a high-resolution TEM (HRTEM) image (Figure 2d) and SAED pattern (Figure 2d inset) provide powerful evidence of the polycrystalline nature of the TiO_2 shell in the composite microspheres. The creation of the mesopores should also be attributed to the tiny slits between neighboring nanocrystals in the shell.

The crystalline structure of the composite microspheres was further investigated using powder X-ray diffraction (PXRD, Figure 3a). Prior to the hydrothermal treatment of the TiO_2 shells, both the MCNCs and Fe_3O_4@TiO_2 microspheres showed a simple PXRD pattern, which was ascribed to the typical cubic structure of Fe_3O_4 (JCPDS 19-629). The lack of a characteristic TiO_2 crystal peak is indicative of an amorphous TiO_2 shell and agrees well with the SAED result. After hydrothermal treatment at 120 °C for 20 h, several new peaks marked "A" were detected for Fe_3O_4@mTiO_2-120. These peaks were indexed to the typical crystallographic planes of anatase-phase TiO_2. The XRD pattern for Fe_3O_4@mTiO_2-80 is significantly different from Fe_3O_4@mTiO_2-120. As observed in Figure 3a, only a weaker peak of TiO_2 was observed at the 2θ value of 25.1°, corresponding to reflections of the (101) crystalline plane. By combining the results of SAED and PXRD, the nanocrystals in the shell of Fe_3O_4@mTiO_2-80 may be too small for easy detection using PXRD, while the products with larger nanocrystals in their shells (Fe_3O_4@mTiO_2-160 and Fe_3O_4@mTiO_2-120) have significantly stronger peak intensities. Further, we can propose a possible hypothesis: a higher reaction temperature leads to the formation of larger nanocrystals, which in turn, produce a larger gap between neighboring nanocrystals. A vibrating sample magnetometer (VSM) (Figure 3b) was employed to identify the magnetic properties and composition of the Fe_3O_4@mTiO_2-80. No

dx.doi.org/10.1021/am501339e | ACS Appl. Mater. Interfaces 2014, 6, 6290−6299

obvious magnetic hysteresis loops (Hc < 30 Oe) were observed for the three types of microspheres based on the field-dependent magnetization plots in the inset of Figure 3b, which indicates that all products possessed superparamagnetic features at room temperature. By comparing the saturation magnetization (Ms) value before and after coating of the TiO_2 layers, the TiO_2 content of the composite microspheres was estimated to be as high as 71 and 69 wt % for Fe_3O_4@TiO_2 and Fe_3O_4@$mTiO_2$-80, respectively. The high TiO_2 content, together with the ultrahigh specific surface area, endows the Fe_3O_4@$mTiO_2$-80 with a probable high enrichment capacity for phosphopeptides. Additionally, the high magnetic susceptibility caused by the cores with high magnetic response values makes the separation of the phosphopeptide-captured microspheres significantly easier and more efficient using magnetic separation. Otherwise, it would require high-speed centrifugation, and proteins with high molecular weights or poor solubility would sediment during this process.

3.2. Investigation of the Phosphopeptide Enrichment Ability of Fe_3O_4@$mTiO_2$-80. The requirement of the material used for phosphopeptidome can be summarized by the following two points: (1) the material should have high selectivity toward phosphopeptide enrichment and (2) the material should have an appropriate pore size to realize the size exclusion effect. A phosphopeptidome study using Fe_3O_4@$mTiO_2$-80 is illustrated in Scheme 2. When both proteins and peptides were mixed with Fe_3O_4@$mTiO_2$-80, the proteins, including the phosphoproteins, were excluded by the entrance of the pore due to the size exclusion effect, while peptides were allowed to penetrate into the pore channel. Aided by the strong interaction between TiO_2 and the phosphoric acid group, the phosphopeptides were anchored onto the surface of the TiO_2 nanocrystals, allowing the other peptides to be washed away. Using magnetic separation, the phosphopeptide-captured microspheres could be isolated from the mixture, and then, the adsorbed phosphopeptides could be desorbed for further analysis.

To test the specificity of Fe_3O_4@$mTiO_2$-80 in the phosphopeptide enrichment process, tryptic digests of standard phosphoprotein β-casein mixed with digests of standard non-phosphoprotein BSA at a molar ratio of 1:500 (with an initial concentration of β-casein at 100 fmol/μL) were used as a test sample. The standard phosphoprotein β-casein harbors three phosphorylated sites and generates three phosphopeptides after trypsin digestion with m/z at 2061.83, 2556.09, and 3122.27 in the MALDI spectrum. In a typical enrichment procedure, the β-casein and BSA digests were first dissolved in a 100 μL loading buffer consisting of 50% acetonitrile containing 5% trifluoroacetic acid (TFA) and were then incubated with Fe_3O_4@$mTiO_2$-80. Afterward, the Fe_3O_4@$mTiO_2$-80 with the captured phosphopeptides were separated from the mixed solution using an external magnetic field, and the phosphopeptides were washed with the loading buffer several times to remove nonspecifically adsorbed peptides. Finally, the phosphopeptides were eluted from the Fe_3O_4@$mTiO_2$-80 with 10 μL of 5% $NH_3 \cdot H_2O$, and 1 μL of this solution was used for MALDI-TOF MS analysis. Before enrichment, the spectrum was dominated by nonphosphopeptides, and no phosphopeptides were detected (Figure 4a). After the selective enrichment process, signals of the three phosphopeptides were easily detected with a clean background, as shown in Figure 4b. This result confirmed the high enrichment selectivity of Fe_3O_4@$mTiO_2$-80 toward phosphopeptides.

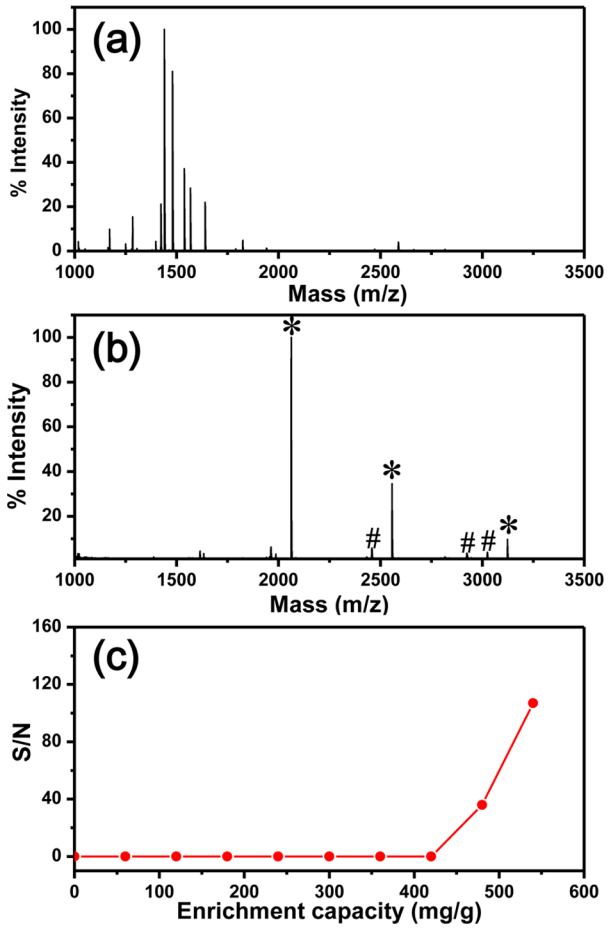

Figure 4. MALDI mass spectra of the tryptic digest mixture of β-casein and BSA (with a molar ratio of β-casein to BSA of 1:500) for the (a) direct analysis and (b) analysis after enrichment using Fe_3O_4@$mTiO_2$-80. "*" and "#" indicate phosphopeptides and their dephosphorylated counterparts, respectively. (c) The enrichment capacity analysis of Fe_3O_4@$mTiO_2$-80.

It is well known that biologically active peptides exist in extremely low abundances. Therefore, the enrichment sensitivity of Fe_3O_4@$mTiO_2$-80 was investigated. To determine the limit of detection (LOD), the loading amount of β-casein was decreased to the amount at which the S/N just exceeded 3. The enrichment sensitivity was determined as 5 fmol·μL^{-1}, as illustrated in the MALDI mass spectrum, Figure S1, Supporting Information. We also compared the selectivity and sensitivity of this method with previous reports given in phosphopeptidome research. The selectivity of this method is significantly better than those previously reported,[41] and the sensitivity is similar.[42] The enrichment capacity and the post-enrichment recovery of the Fe_3O_4@$mTiO_2$-80 composite microspheres toward phosphopeptides were further evaluated. The enrichment capacity of Fe_3O_4@$mTiO_2$-80 for phosphopeptides was 480 mg·g^{-1} (Figure 4c). The high enrichment capacity can be attributed to the high TiO_2 content and the extremely high surface area (>600 m^2/g). The recovery of phosphopeptides from Fe_3O_4@$mTiO_2$-80 was evaluated at 81% using an isotope labeling method (Figure S2, Supporting Information), which was satisfactory for phosphopeptide extraction. On the basis of these tests, we conclude that the Fe_3O_4@$mTiO_2$-80 microspheres act as an ideal adsorbent for phosphopeptides.

dx.doi.org/10.1021/am501339e | ACS Appl. Mater. Interfaces 2014, 6, 6290−6299

3.3. Size Exclusion Capability of Fe_3O_4@mTiO_2-80. To confirm the size exclusion capability of Fe_3O_4@mTiO_2-80, a tryptic digest of β-casein was mixed into a protein mixture that included a standard phosphoprotein (β-casein, molecular weight of 24 kDa), a standard nonphosphoprotein (BSA, molecular weight of 66 kDa), and a standard nonphosphoprotein (cytochrome c from horse heart, molecular weight 11 kDa) with a mass ratio of 1:100:100:100 (initial concentration of β-casein at 10 ng/μL). Before enrichment, the mixture was directly analyzed using MALDI-MS, and the signals of any phosphopeptides were too weak for detection because of the interference of significant amounts of protein (Figure 5a). After enrichment, the phosphopeptides eluted from the Fe_3O_4@mTiO_2-80 were subjected to mass spectrometric analysis. As the mass spectrum revealed, the phosphopeptides were selectively removed from the protein mixture (Figure 5b). To further verify the size-exclusion capability, we selected two types of phosphoproteins with different molecular weights (the molecular weights for asialofetuin and β-casein are 48 and 24 kDa, respectively) and measured their adsorption on Fe_3O_4@mTiO_2-80. As observed in Table 1, the adsorption capacity of Fe_3O_4@mTiO_2-80 for β-casein is 57.0 mg·g^{-1}, whereas this value for asialofetuin is only 3.6 mg·g^{-1}. The reason for this result is the fact that the molecular weight of asialofetuin is approximately twice that of β-casein. Therefore, it was impossible for asialofetuin to pass through the pores, whereas small amounts of β-casein were able to pass into the pore channels. The experimental results were also compared with the theoretical sizes of these proteins. In the literature, it has been reported that the radius of gyration (Rg) of the phosphorylated protein β-casein is 4.6 nm.[43] The molecular weight (MW) of β-casein (M_1) is approximately 24,000. The MW of asialofetuin (M_2) is approximately 48,000, and the size of asialofetuin can be calculated from the Flory formula $Rg \propto M^{3/5}$. Hence, Rg for asialofetuin $Rg_2 \approx Rg_1 \times (M_2/M_1)^{3/5}$ can be calculated as approximately 7 nm. Therefore, the diameters of β-casein and asialofetuin are approximately 9.2 and 14 nm, respectively. Additionally, because asialofetuin is also a glycoprotein with branched glycan chains, its actual size is likely larger than the theoretical size. The above data are the theoretical sizes of these proteins; further, the sizes of proteins are affected by other conditions, such as solvent, temperature, etc. Our experiments showed that higher amounts of adsorption were obtained for smaller phosphoproteins, and these results were generally consistent with the differences in the theoretical sizes of the molecules. The adsorption capacity of Fe_3O_4@mTiO_2-160 can provide additional powerful evidence for the size-exclusion capability of Fe_3O_4@mTiO_2-80. Because the pore size (8.6 nm) is larger than the size of either β-casein or asialofetuin, Fe_3O_4@mTiO_2-160 has a relatively large capacity for both β-casein and asialofetuin (134.4 and 67.6 mg·g^{-1}, respectively). Although Fe_3O_4@mTiO_2-80 can also adsorb a few low-molecular-weight phosphoproteins, its adsorption capacity for phosphoproteins is significantly lower than its adsorption capacity for phosphopeptides (480 mg·g^{-1}). The above results clearly indicate that Fe_3O_4@mTiO_2-80 possesses the desired size-exclusion capability against the proteins, including both nonphosphoproteins and phosphoproteins.

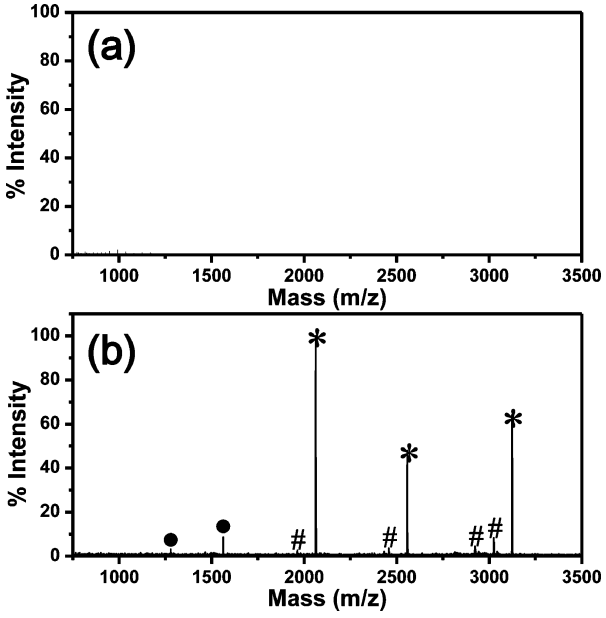

Figure 5. MALDI mass spectra of the tryptic digest of β-casein in the mixture of proteins containing β-casein, BSA, and cytochrome C with a mass ratio of 1:100:100:100, (a) before and (b) after enrichment with Fe_3O_4@mTiO_2-80. "∗", "#", and "●" indicate phosphorylated peptides, their dephosphorylated counterparts, and double charged counterparts, respectively.

3.4. Highly Specific Revelation of the Phosphopeptidome of Snake Venom. To further apply our method to the analysis of the phosphopeptidome in real samples, we chose to analyze snake venom. As a complex mixture of proteins, peptides, and other components, such as metallic cations, carbohydrates, nucleosides, etc., the snake venom peptidome is a rich and valuable resource for drug discovery.[44,45] Nevertheless, despite the progresses made in snake venom peptidome research, the phosphopeptidome of snake venom has rarely been studied. Herein, we enrich the phosphopeptidome in snake venom using Fe_3O_4@mTiO_2-80. After treatment with Fe_3O_4@mTiO_2-80 microspheres, the phosphopeptidome was enriched on the inner surface of the pores, while larger proteins, including phosphoproteins, were excluded. The phosphopeptides eluted from the microspheres were dried thoroughly using a vacuum centrifuge and then redissolved in an aqueous solution of 5% ACN containing 0.1% formic acid, separated using nano-LC, and analyzed using online ESI-MS/MS. After a database search, the peptide sequences were obtained. A representative spectrum is shown in Figure S3, Supporting Information. A total of 35 phosphopeptides were identified (Table S1, Supporting Information), accounting for 75% of the

Table 1. Comparison of the Material Properties of Two Types of Fe_3O_4@mTiO_2 and Their Adsorption Capacities for Asialofetuin and β-Casein

Fe_3O_4@mTiO_2	pore size (nm)	adsorption capacity for β-casein (mg·g^{-1})	adsorption capacity for asialofetuin (mg·g^{-1})
Fe_3O_4@mTiO_2-80	3.4	57.0	3.6
Fe_3O_4@mTiO_2-160	8.6	134.4	67.6

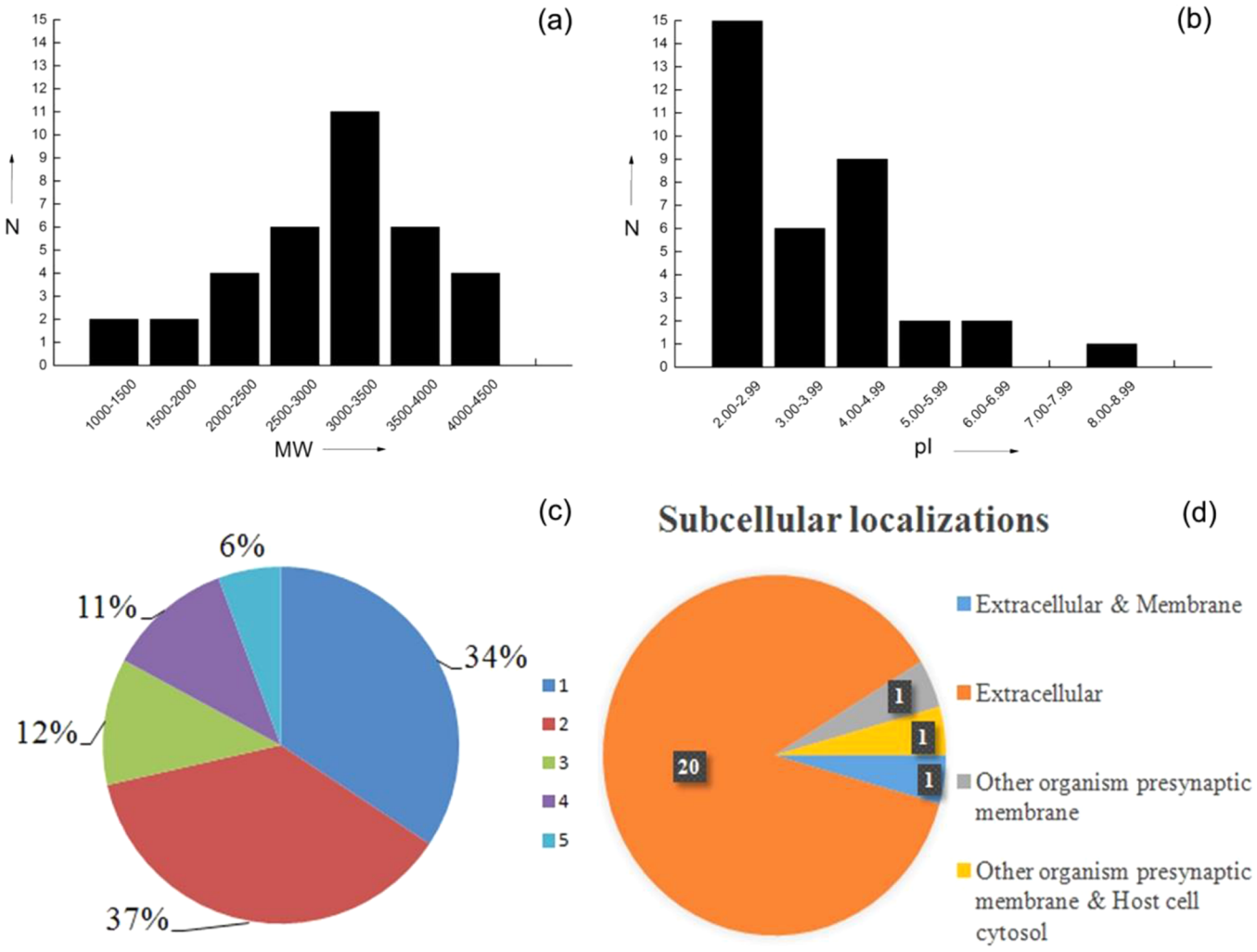

Figure 6. Peptide abundances within different (a) MW, (b) pI ranges (N = peptide number), and (c) phosphorylated sites (the numerals 1−5 denote the number of phosphorylated sites on each phosphopeptide). (d) The subcellular locations of the corresponding precursor proteins.

total identified peptides. Figure 6a shows that all of the identified phosphopeptides had molecular weights ranging from 1,000 to 5,000 Da, which is consistent with the size-exclusion effect. Figure 6b shows that the pI values of most phosphopeptides range from 2.0 to 4.0 because the negatively charged phospho-group decreases the pI of the peptides. Additionally, we noticed that the identified phosphopeptides harbored between one and five phosphorylated sites (Figure 6c), which suggests that Fe_3O_4@mTiO_2-80 was able to efficiently capture phosphopeptides with one or more phosphorylated sites. This fact further indicates the universality of this extraction method toward phosphopeptidome. Finally, we analyzed the subcellular locations of these identified phosphopeptides according to their precursor proteins. These 35 phosphopeptides correspond to 23 precursor proteins. All of these precursor proteins were annotated as secreted proteins (Figure 6d). The subcellular locations are in accordance with previous results because the proteins in the snake venom are secreted from the gland. Among the 23 proteins, 16 precursor proteins exist at the protein level, and 7 precursor proteins are present at the transcriptional level. For example, the precursor protein of these three identified phosphopeptides K.pTpSTHIAPLSLPSSPPSVGSVCRIM*GWGpTVpT.S, N.RPVKTSpTHIAPLpSLPpSpSPPpSVGSVCRIM*GWGTVTSPN.E, K.NYpTKWDKDIM*LIKLNRPVKpTpSpTHIAPLpS.L is Serine protease VLSP-3. This protein is present at the transcriptome level in the venom gland of *Macrovipera lebetina*. These experimentally identified phosphopeptides provided the experimental basis for the existence of Serine protease VLSP-3 at the protein level with the 105th, 122nd, 123rd, 124th, 130th, 133rd, 134th, 137th, 149th, and 151st sites of the amino acid sequence as the phosphorylated sites.

4. CONCLUSIONS

In summary, magnetic mesoporous titania microspheres (Fe_3O_4@mTiO_2-80) with a well-defined core/shell structure were successfully synthesized by directly coating amorphous titania onto the surface of MCNCs, followed by a hydrothermal process at 80 °C. The temperature of the hydrothermal treatment is critical for converting the amorphous titania shell into a crystalline structure with the desired pore diameter (3.4 nm) and a narrow pore size distribution. Moreover, the resulting products also have prominent specific surface areas (as high as 603.5 m^2/g) and high magnetic susceptibilities. By utilizing these features, Fe_3O_4@mTiO_2-80 selectively extracted low-abundance phosphopeptides from complicated samples containing large amounts of proteins and nonphosphopeptides. By applying this approach, we successfully identified 35

phosphopeptides in a real sample of snake venom, which accounted for 75% of the total identified peptides.

■ ASSOCIATED CONTENT

Supporting Information

Enrichment capacity of Fe_3O_4@mTiO_2 towards phosphopeptides and phosphoproteins, enrichment sensitivity of Fe_3O_4@mTiO_2 towards phosphopeptides, enrichment recovery of Fe_3O_4@mTiO_2 towards phosphopeptides, and representative MS/MS spectrum of the phosphopeptide. This material is available free of charge via the Internet at http://pubs.acs.org.

■ AUTHOR INFORMATION

Corresponding Authors

*E-mail: ccwang@fudan.edu.cn.

*E-mail: luhaojie@fudan.edu.cn.

Author Contributions

‡Y.Z. and W.M. contributed equally.

Notes

The authors declare no competing financial interest.

■ ACKNOWLEDGMENTS

This work was supported by the National Science and Technology Key Project of China (2012CB910602, 2012AA020204, and 2012CB910103), the National Science Foundation of China (Grant Nos. 21025519, 51073040, and 21335002), and Shanghai Projects (Grants Eastern Scholar, 11XD1400800, 13520720200, and B109).

■ REFERENCES

(1) Kresge, C. T.; Leonowicz, M. E.; Roth, W. J.; Vartuli, J. C.; Beck, J. S. Ordered Mesoporous Molecular-Sieve Synthesized by a Liquid-Crystal Mechanism. *Nature* **1992**, *359*, 710−712.

(2) Beck, J. S.; Vartuli, J. C.; Roth, W. J.; Leonowicz, M. E.; Kresge, C. T.; Schmitt, K. D.; Chu, C. T. W.; Olson, D. H.; Sheppard, E. W.; McCullen, S. B.; Higgins, J. B.; Schlenker, J. L. A New Family of Mesoporous Molecular-Sieves Prepared with Liquid-Crystal Templates. *J. Am. Chem. Soc.* **1992**, *114*, 10834−10843.

(3) Zhao, D. Y.; Feng, J. L.; Huo, Q. S.; Melosh, N.; Fredrickson, G. H.; Chmelka, B. F.; Stucky, G. D. Triblock Copolymer Syntheses of Mesoporous Silica with Periodic 50 to 300 Angstrom Pores. *Science* **1998**, *279*, 548−552.

(4) Scott, B. J.; Wirnsberger, G.; Stucky, G. D. Mesoporous and Mesostructured Materials for Optical Applications. *Chem. Mater.* **2001**, *13*, 3140−3150.

(5) Zhou, H. S.; Li, D. L.; Hibino, M.; Honma, I. A Self-Ordered, Crystalline-Glass, Mesoporous Nanocomposite for Use as a Lithium-Based Storage Device with Both High Power and High Energy Densities. *Angew. Chem., Int. Ed.* **2005**, *44*, 797−802.

(6) Vallet-Regi, M.; Balas, F.; Arcos, D. Mesoporous Materials for Drug Delivery. *Angew. Chem., Int. Ed.* **2007**, *46*, 7548−7558.

(7) Lee, C. H.; Lin, T. S.; Mou, C. Y. Mesoporous Materials for Encapsulating Enzymes. *Nano Today* **2009**, *4*, 165−179.

(8) Lee, J. E.; Lee, N.; Kim, T.; Kim, J.; Hyeon, T. Multifunctional Mesoporous Silica Nanocomposite Nanoparticles for Theranostic Applications. *Acc. Chem. Res.* **2011**, *44*, 893−902.

(9) Wu, Z. X.; Zhao, D. Y. Ordered Mesoporous Materials as Adsorbents. *Chem. Commun.* **2011**, *47*, 3332−3338.

(10) Perego, C.; Millini, R. Porous Materials in Catalysis: Challenges for Mesoporous Materials. *Chem. Soc. Rev.* **2013**, *42*, 3956−3976.

(11) Tian, R. J.; Zhang, H.; Ye, M. L.; Jiang, X. G.; Hu, L. H.; Li, X.; Bao, X. H.; Zou, H. F. Selective Extraction of Peptides from Human Plasma by Highly Ordered Mesoporous Silica Particles for Peptidome Analysis. *Angew. Chem., Int. Ed.* **2007**, *46*, 962−965.

(12) Xu, Y. W.; Wu, Z. X.; Zhang, L. J.; Lu, H. J.; Yang, P. Y.; Webley, P. A.; Zhao, D. Y. Highly Specific Enrichment of Glycopeptides Using Boronic Acid-Functionalized Mesoporous Silica. *Anal. Chem.* **2009**, *81*, 503−508.

(13) Lu, Z. D.; Ye, M. M.; Li, N.; Zhong, W. W.; Yin, Y. D. Self-Assembled TiO_2 Nanocrystal Clusters for Selective Enrichment of Intact Phosphorylated Proteins. *Angew. Chem., Int. Ed.* **2010**, *49*, 1862−1866.

(14) Sun, Z. K.; Deng, Y. H.; Wei, J.; Gu, D.; Tu, B.; Zhao, D. Y. Hierarchically Ordered Macro-/Mesoporous Silica Monolith: Tuning Macropore Entrance Size for Size-Selective Adsorption of Proteins. *Chem. Mater.* **2011**, *23*, 2176−2184.

(15) Qin, H. Q.; Gao, P.; Wang, F. J.; Zhao, L.; Zhu, J.; Wang, A. Q.; Zhang, T.; Wu, R.; Zou, H. F. Highly Efficient Extraction of Serum Peptides by Ordered Mesoporous Carbon. *Angew. Chem., Int. Ed.* **2011**, *50*, 12218−12221.

(16) Gu, Z. Y.; Chen, Y. J.; Jiang, J. Q.; Yan, X. P. Metal-Organic Frameworks for Efficient Enrichment of Peptides with Simultaneous Exclusion of Proteins from Complex Biological Samples. *Chem. Commun.* **2011**, *47*, 4787−4789.

(17) Kim, J.; Piao, Y.; Lee, N.; Park, Y. I.; Lee, I. H.; Lee, J. H.; Paik, S. R.; Hyeon, T. Magnetic Nanocomposite Spheres Decorated with NiO Nanoparticles for a Magnetically Recyclable Protein Separation System. *Adv. Mater.* **2010**, *22*, 57−60.

(18) Shao, M. F.; Ning, F. Y.; Zhao, J. W.; Wei, M. D.; Evans, G.; Duan, X. Preparation of Fe_3O_4@SiO_2@Layered Double Hydroxide Core-Shell Microspheres for Magnetic Separation of Proteins. *J. Am. Chem. Soc.* **2012**, *134*, 1071−1077.

(19) Ma, W. F.; Zhang, Y.; Li, L. L.; Zhang, Y. T.; Yu, M.; Guo, J.; Lu, H. J.; Wang, C. C. Ti^{4+}-Immobilized Magnetic Composite Microspheres for Highly Selective Enrichment of Phosphopeptides. *Adv. Funct. Mater.* **2013**, *23*, 107−115.

(20) Ma, W. F.; Li, L. L.; Zhang, Y.; An, Q.; You, L. J.; Li, J. M.; Zhang, Y. T.; Xu, S.; Yu, M.; Guo, J.; Lu, H. J.; Wang, C. C. Ligand-Free Strategy for Ultrafast and Highly Selective Enrichment of Glycopeptides Using Ag-Coated Magnetic Nanoarchitectures. *J. Mater. Chem.* **2012**, *22*, 23981−23988.

(21) Zhang, L.; Qiao, S. Z.; Jin, Y. G.; Yang, H. G.; Budihartono, S.; Stahr, F.; Yan, Z. F.; Wang, X. L.; Hao, Z. P.; Lu, G. Q. Fabrication and Size-Selective Bioseparation of Magnetic Silica Nanospheres with Highly Ordered Periodic Mesostructure. *Adv. Funct. Mater.* **2008**, *18*, 3203−3212.

(22) Liu, J.; Qiao, S. Z.; Hu, Q. H.; Lu, G. Q. Magnetic Nanocomposites with Mesoporous Structures: Synthesis and Applications. *Small* **2011**, *7*, 425−443.

(23) Liu, S. S.; Chen, H. M.; Lu, X. H.; Deng, C. H.; Zhang, X. M.; Yang, P. Y. Facile Synthesis of Copper(II)Immobilized on Magnetic Mesoporous Silica Microspheres for Selective Enrichment of Peptides for Mass Spectrometry Analysis. *Angew. Chem., Int. Ed.* **2010**, *49*, 7557−7561.

(24) Liu, Z.; Li, M.; Yang, X. J.; Yin, M. L.; Ren, J. S.; Qu, X. G. The Use of Multifunctional Magnetic Mesoporous Core/Shell Heteronanostructures in a Biomolecule Separation System. *Biomaterials* **2011**, *32*, 4683−4690.

(25) Ma, W. F.; Zhang, Y.; Li, L. L.; You, L. J.; Zhang, P.; Zhang, Y. T.; Li, J. M.; Yu, M.; Guo, J.; Lu, H. J.; Wang, C. C. Tailor-Made Magnetic Fe_3O_4@mTiO_2 Microspheres with a Tunable Mesoporous Anatase Shell for Highly Selective and Effective Enrichment of Phosphopeptides. *ACS Nano* **2012**, *6*, 3179−3188.

(26) Wu, J. H.; Li, X. S.; Zhao, Y.; Gao, Q. A.; Guo, L.; Feng, Y. Q. Titania Coated Magnetic Mesoporous Hollow Silica Microspheres: Fabrication and Application to Selective Enrichment of Phosphopeptides. *Chem. Commun.* **2010**, *46*, 9031−9033.

(27) Cheng, G.; Zhang, J. L.; Liu, Y. L.; Sun, D. H.; Ni, J. Z. Synthesis of Novel Fe_3O_4@SiO_2@CeO_2 Microspheres with Mesoporous Shell for Phosphopeptide Capturing and Labeling. *Chem. Commun.* **2011**, *47*, 5732−5734.

(28) Robinson, W. H.; Steinman, L. Human Peptidome Display. *Nat. Biotechnol.* **2011**, *29*, 500−502.

(29) Petricoin, E. F.; Belluco, C.; Araujo, R. P.; Liotta, L. A. The Blood Peptidome: A Higher Dimension of Information Content for Cancer Biomarker Discovery. *Nat. Rev. Cancer* **2006**, *6*, 961−967.
(30) Liotta, L. A.; Ferrari, M.; Petricoin, E. Written in Blood. *Nature* **2003**, *425*, 905.
(31) Deribe, Y.L.; Pawson, T.; Dikic, I. Post-Translational Modifications in Signal Integration. *Nat. Struct. Mol. Biol.* **2010**, *17*, 666−672.
(32) Hu, L. H.; Ye, M. L.; Zou, H. F. Recent Advances in Mass Spectrometry-Based Peptidome Analysis. *Expert Rev. Proteomics* **2009**, *6*, 433−437.
(33) Hu, Y.; Bouamrani, A.; Tasciotti, E.; Li, L.; Liu, X. W.; Ferrari, M. Tailoring of the Nanotexture of Mesoporous Silica Films and Their Functionalized Derivatives for Selectively Harvesting Low Molecular Weight Protein. *ACS Nano* **2010**, *4*, 439−451.
(34) Liu, L. T.; Zhang, Y.; Zhang, L.; Yan, G. Q.; Yao, J.; Yang, P. Y.; Lu, H. J. Highly Specific Revelation of Rat Serum Glycopeptidome by Boronic Acid-Functionalized Mesoporous Silica. *Anal. Chim. Acta* **2012**, *753*, 64−72.
(35) Zhang, L.; Wu, S. B.; Lia, C.; Yang, Q. H. Facile Synthesis of Hybrid Hollow Mesoporous Nanospheres with High Content of Interpenetrating Polymers for Size-Selective Peptides/Proteins Enrichment. *Chem. Commun.* **2012**, *48*, 4190−4192.
(36) Wang, F.; Guan, Y. F.; Zhang, S.; Xia, Y. Hydrophilic Modification of Silica-Titania Mesoporous Materials as Restricted-Access Matrix Adsorbents for Enrichment of Phosphopeptides. *J. Chromatogr., A* **2012**, *1246*, 76−83.
(37) Li, X. S.; Su, X.; Zhu, G. T.; Zhao, Y.; Yuan, B. F.; Guo, L.; Feng, Y. Q. Titanium-Containing Magnetic Mesoporous Silica Spheres: Effective Enrichment of Peptides and Simultaneous Separation of Nonphosphopeptides and Phosphopeptides. *J. Sep. Sci.* **2012**, *35*, 1506−1513.
(38) Li, X. S.; Pan, Y. N.; Zhao, Y.; Yuan, B. F.; Guo, L.; Feng, Y. Q. Preparation of Titanium-Grafted Magnetic Mesoporous Silica for the Enrichment of Endogenous Serum Phosphopeptides. *J. Chromatogr., A* **2013**, *1315*, 61−69.
(39) Qin, H.; Wang, Q. F. J.; Wang, P. Y.; Zhao, L.; Zhu, J.; Yang, Q. H.; Wu, R. A.; Ye, M. L.; Zou, H. F. Phosphoric Acid Functionalized Mesoporous Organo-Silica (EPO) as the Adsorbent for in Situ Enrichment and Isotope Labeling of Endogenous Phosphopeptides. *Chem. Commun.* **2012**, *48*, 961−963.
(40) Ma, W. F.; Xu, S.; Li, J. M.; Guo, J.; Lin, Y.; Wang, C. C. Hydrophilic Dual-Responsive Magnetite/PMAA Core/Shell Microspheres with High Magnetic Susceptibility and pH Sensitivity via Distillation-Precipitation Polymerization. *J. Polym. Sci., Part A: Polym. Chem.* **2011**, *49*, 2725−2733.
(41) Hu, Y.; Peng, Y.; Lin, K.; Shen, H. F.; Brousseau, L. C.; Sakamoto, J.; Sun, T.; Ferrari, M. Surface Engineering on Mesoporous Silica Chips for Enriching Low Molecular Weight Phosphorylated Proteins. *Nanoscale* **2011**, *49*, 2725−2733.
(42) Hu, L. H.; Zhou, H. J.; Li, Y. H.; Sun, S. T.; Guo, L. H.; Ye, M. L.; Tian, X. F.; Guo, J. R.; Yang, S. L.; Zou, H. F. Profiling of Endogenous Serum Phosphorylated Peptides by Titanium (IV) Immobilized Mesoporous Silica Particles Enrichment and MALDI-TOF MS Detection. *Anal. Chem.* **2009**, *81*, 94−104.
(43) Schmidt, D. G.; Payens, T. A. J. Evaluation of Positive and Negative Contributions to Second Virial-Coefficient of Some Milk Proteins. *J. Colloid Interface Sci.* **1972**, *39*, 655−662.
(44) Escoubas, P.; King, G. F. Venomics as a Drug Discovery Platform. *Expert Rev. Proteomics* **2009**, *6*, 221−224.
(45) Tashima, A. K.; Zelanis, A.; Kitano, E. S.; Ianzer, D. R.; Melo, L.; Rioli, V.; Sant'anna, S. S.; Schenberg, A. C. G.; Camargo, A. C. M.; Serrano, S. M. T. Peptidomics of Three Bothrops Snake Venoms: Insights Into the Molecular Diversification of Proteomes and Peptidomes. *Mol. Cell. Proteomics* **2012**, *11*, 1245−1262.